Engenharia Agrícola

ISSN: 1809-4430 (on-line)

www.engenhariaagricola.org.br

Scientific Paper
Doi: http://dx.doi.org/10.1590/1809-4430-Eng.Agric.v44e20240039/2024

DESIGN AND DISCRETE ELEMENT SIMULATION OF A BIOMIMETIC WEEDING DEVICE MODELLED ON A CRAB CLAW TOE

Jianguo Meng[1*], Fangxu Li[1], Zheng Li[1], Weidong Xian[1], Jianjun Li[1]

[1*]Corresponding author. Inner Mongolia University of Science and Technology/Baotou, China.
E-mail: mjg101@163.com | ORCID ID: https://orcid.org/0000-0002-0385-1607

KEYWORDS

crab claw toe, bionic weeding claw, discrete element, inverse reconstruction, joint simulation.

ABSTRACT

As weeds cannot be eradicated in corn fields, a crab claw toe was used as the research object and combined with the agronomic requirements of corn fields to design a bionic weed claw suitable for corn fields. The contour curve of the crab claw toe was extracted and fitted through the Matlab image processing technology and fitting tool to establish a bionic claw finger 3D model using Solid works. According to the mechanical soil dynamics theory of dynamics analysis, the root–soil aggregates are easily broken, loosened, and drained under the action of the bionic claw fingers. Based on single image inverse reconstruction technology, the weed root system–soil aggregates discrete meta-model was established. Recur Dyn was used in the bionic weed claw kinematics simulation to verify the reliability of the movement of the mechanism and to realise the expected action of the weeding operation. We analysed the movement speed, displacement, and trajectory of soil particles in different depth layers through the joint simulation and comparison test. Using the mechanism of weeding and resistance reduction of the bionic weeding claw, under the same working conditions, the average resistance reduction rate of the bionic claw finger compared with the flat claw finger in the grasping process was 16.4%. The resistance of grass roots was reduced 23.3%, making it easier to pull out the more intact grass roots.

INTRODUCTION

As one of the most in-demand cereal food crops, maize requires field weeding, especially for field weeds that severely threaten its growth (Shen, 2021). Currently, field weeding mainly relies on pesticides and mechanical ploughs or cutters for treatment but often causes problems such as environmental pollution, destruction of soil structure, and inability to eradicate grass roots. Therefore, weeding machinery in corn fields must be improved. The performance of the weeding component, which is the actuator of weeding machinery, is critical because it is responsible for removing the weeds (Cordill & Grift, 2011; Bo et al., 2022).

With the improvement of the scientific and technological level of agricultural machinery, both domestic and foreign scholars have adopted the discrete element method and the multidisciplinary crossover of bionics to explore how the interactions between bionic structures and microscopic particles affect the overall system and how these principles can be applied to the field of weed control technology (Zeng et al., 2021). Xu et al. (2023) analysed the physical and mechanical properties of standard weed root systems in oil tea forests combined with the movement of the tool, designed a vertical spiral tillage knife, and used the discrete element method to establish a root–soil complex model to study the effect of the tool on the weed root system in terms of disturbance, soil fragmentation, and root removal. The pecten scallop flap was used as a biomimetic prototype for the bionic design of the weeding wheel. Du et al. (2023) simulated and analysed the interaction between the weeding wheel and the soil, effectively reducing resistance during the weeding operation and reducing the soil adhesion phenomenon. A 3D scanner and frozen section method has been used to determine the contour lines of the paw toes of flat moles and fit them to a bionic biplane weeding shovel. Yin (2022) used the discrete element method to verify that bionic edges cut weeds better than traditional straight edges. Yang et al. (2021) analysed the multi-toe combination of

[1] Inner Mongolia University of Science and Technology/Baotou, China.

Area Editor: Fábio Lúcio Santos
Received in: 3-8-2024
Accepted in: 4-29-2024

structural features of the forelimb palm of the mole rat to determine the mathematical model of its structure and designed a bionic soil-cutting blade; the tested bionic blade had better soil-cutting performance and reduced the resistance of soil tillage. The growth of weeds in corn fields is complex, and the existing weed control methods are mainly based on cutting or turning the grass roots, which makes it challenging to meet the needs of weed eradication operations in corn fields.

As a result, this study designed a bionic claw finger and extended it use as a bionic weeding claw by combining the use of discrete elements, multi-body dynamics, and bionics to carry out weed-pulling work in a narrow and ever-changing corn field. This study established a model of restored real grass roots based on the single-image inverse reconstruction technique, showed a discrete element model of agglomerates generated from the root system of the weed and the soil, analysed the bionic claw finger to reduce the damping and loosening of the soil mechanism through mechanical analysis, and carried out joint simulation experiments to validate the working performance of the bionic weeding claw.

MATERIAL AND METHODS

Measurement of crab claw toe geometry

Ten test samples of river crabs were randomly selected, and the four claw toes on the same side were measured separately. The macroscopic dimensions of the claw toes mainly included the claw toe length L (mm), claw toe thickness T (mm), and claw toe height H (mm), as shown in Figure 2, and a reasonable design of the bionic claw finger structure was carried out through the measurement of these characteristic parameters. The measuring instrument was a vernier calliper with an accuracy of 0.01 mm. The measured parameters were counted and averaged; the statistical results are shown in Figure 1.

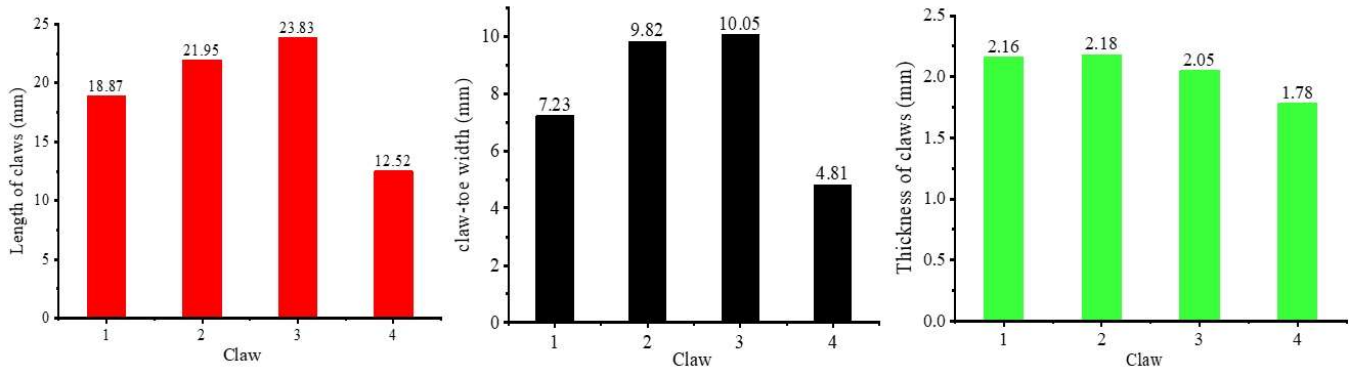

FIGURE 1. Parameters of claw toe dimensions.

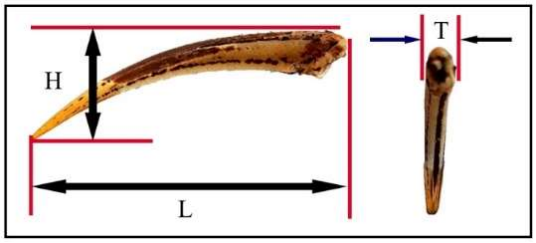

FIGURE 2. Parametric division of claw toe dimensions.

Determination of field physical parameters and discrete element modelling

Determination of soil physical parameters: Corn was grown to the 3–5 leaf stage, and weeds were spread on the ridge and the two sides of the soil ridge. This study evaluated the distribution of weeds between plants, and soil sampling and analysis only occurred on the ridge. To ensure the accuracy of the experimental data, 10 groups of soil samples were collected in the maize experimental field for soil sampling and measurement of soil density and soil particle size (Yang et al., 2021; Hai et al., 2023). Measuring tools included a ring soil extractor, electronic scale (accuracy of 0.1 g), and test separation sieve. The results of the test measurements were counted, as shown in Table 1. Soil density was calculated using the following formula.

$$\rho = \frac{m}{v} \quad (1)$$

Where:

m - soil mass (g);

v - soil volume (cm³).

TABLE 1. Statistical results of soil density.

Serial	Mass (g)	Volume (cm^3)	Density (g/cm^3)
1	129.7	100	1.297
2	138.5	100	1.385
3	130.2	100	1.302
4	132.8	100	1.328
5	141.6	100	1.416
Average			1.346

TABLE 2. Distribution of soil particle diameter.

Particle diameter (mm)	≤0.1	0.1–0.5	0.5–1	1–2	≥2
Percentage (%)	12	21	49	13	5

Soil discrete element modelling: The discrete element method (DEM) for establishing the soil model can show a more realistic response to the movement of soil particles. Based on the determination of the physical parameters, particle properties, and contact parameters, the combination of soil particle shapes were spherical (≤0.5 mm), cylindrical (0.5–1 mm), irregular polygonal shape (1–2 and ≥2 mm). In the EDEM software, the spherical particles can be stacked and combined to form arbitrary polygons. Thus, the spherical particles were used for stacking and filling. The radius of the filled particles was 0.5 mm, and the radii of the spliced particles were 0.25, 0.5, 1, 2, and ≥2 mm. Stacking of the particles is shown in Figure 3.

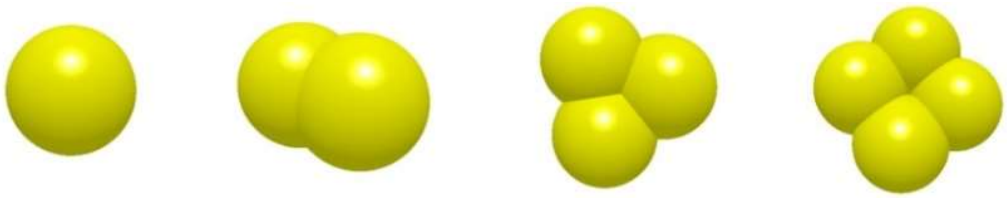

a. Monospherical b. Bispherical c. Triangular d. Cubic

FIGURE 3. Soil particle accumulation model.

Soil particles have nonlinear mobility, and with the moisture in the soil and the mucus secreted by plants, there is adhesion and solid-like properties between soil particles. The interaction force between soils becomes very small after the rupture of soil blocks. The contact characteristics between soil particles align with the Hertz–Mindlin (no slip) contact theory, and the additional Bonding V2 contact considers the effect of the inter-particle bonding contact force. Therefore, in this study, Hertz–Mindlin, with Bonding V2, was chosen as the contact model between soils, and the soil-like solid properties were restored.

Grass roots discrete element modelling: Weed root systems form stable root–soil hybrid aggregates through physical interactions with the soil during growth. This is because the root system can gradually form larger particles or clumps in the surrounding small soil particles using processes, including compression and entanglement. At the same time, the weed roots reduce the water content of the soil around the inter-root zone by absorbing water from the soil, which in turn increases soil stability (Tao et al., 2021; Liu et al., 2023). This action can increase the compactness and durability of the soil. Therefore, the physical action of the weed root system is crucial in the study of weed control operations that need to be preceded by an understanding of the process of the formation and stabilisation of soil aggregates (Yang et al., 2021).

In the existing research on root–soil mixtures, the shape of root system modelling is too idealised to fully highlight the intricate physical characteristics of the root system, resulting in a certain gap between the experimental results and the real data. To restore the shape of the weed root system and the interaction between the root system and the soil, we need to consider the influence of the end root system more carefully. The end root system can provide more force to promote the phenomenon of close bonding between the soil and the root system (Qi et al., 2011; Liu et al., 2019). This phenomenon is important for weed removal operations and should not be ignored.

To reconstruct the real model of real weed roots, the traditional construction method is to use a laser scanner to obtain a 3D point cloud and carefully take many photographs from different views around the real weed roots, which is accurate but complicated to perform and requires high equipment accuracy (Zeng et al., 2023). In this study, the grass root reconstruction technique based on a single image was used to reverse model the weed root system. Reverse reconstruction technology can determine the appearance characteristics of physical objects, and the realisation principle can be summarised as follows: obtain the complete distribution of grass roots and record the direction of the distribution of branches and trunks, depict the 2D distribution characteristics in the form of line sketches, collect the node positions of the original trunk and main branches and the

radius size of the node positions, use conditional generation of the adversarial network to extract the user-drawn simple 2D line sketches, and infer the 3D contour and skeleton of grass roots by combining them with the node data. Based on the predicted 3D contour and skeleton, the programmed reverse reconstruction technique can be used to generate a morphologically realistic grass root model. (Liu et al., 2021).

Grass root systems have more complex and rich branching systems. After deep neural networks predicted the basic 3D shape of the root system, detailed root models were generated through procedural modelling. The specific operation was as follows: take a group of the weed root systems to depict its morphological characteristics, record the average radius size of the main root and the distribution of branches, run the recorded information in the programme, set the number of iterations to 1, the degree of iterative bending is 0.0007, the base trunk radius is 2.5 mm, the radius contraction rate is 90% based on the morphological characteristics of the roots of the grass and the distribution of the branches of the sketches, mark the trunk and branch areas, generate a 2D frame, observe the expected results, establish a 3D frame and iterative generation, and output the corresponding skeleton and contour depth images. The application of procedural modelling methods to generate a weed root model within the contour-defined shape was based on the predicted trunk skeleton. Finally, the established weed root model was imported into EDEM software for particle filling with 571 particles, as shown in Figure 4.

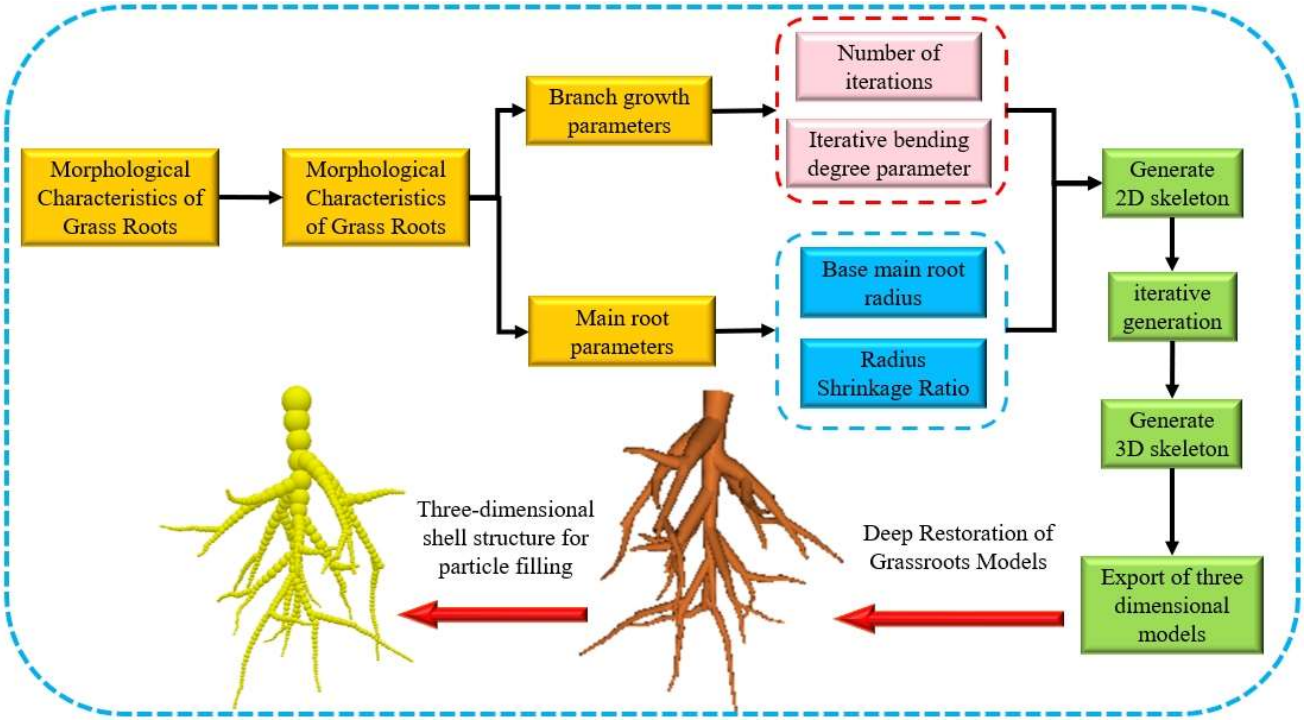

FIGURE 4. Grass root modelling.

As the field soil is affected by the environment, the surface soil is more prone to water and nutrient loss than the inner soil, resulting in higher outer soil hardness than the inner soil; solid inner and outer soil need to be generated separately. To reduce parameter calibration, based on Cao et al. (2023) and Fan (2020), the following parameters were set: normal ultimate stress between the outer and outer soil layers, 25,000 Pa; tangential ultimate stress, 15,000 Pa; normal stiffness, 2.5e+06 N/m^3; shear stiffness, 1.5e+06 N/m^3; normal ultimate stress between the outer and outer soil layer 23,000 Pa; tangential ultimate stress, 13,000 Pa; normal stiffness, 2.5e+06 N/m^3; and shear stiffness, 1.5e+06 N/m^3. Xiao et al. (2021) and Li et al. (2023) set the contact coefficients between the soil, grass roots, and soil-touching components, and the specific values are shown in Tables 3 and 4.

TABLE 3. Parameters of the EDEM model.

Parameter name	Parameter value
Poisson ratio for claw fingers	0.5
Density of claw finger material / (kg/m^3)	7850
Shear modulus of claw finger / Pa	2.1e+11
Poisson ratio for soil	0.4
Soil density / (kg/m^3)	1346
Shear modulus of soil (outer layer) / Pa	2.1e+06
Shear modulus of soil (inner layer) / Pa	1e+06
Grass root Poisson ratio	0.52
Grass root density / (kg/m^3)	1070
Grass root shear modulus	9.8e+04
Normal stiffness per unit area / (N/m^3)	2.5e+06
Shear stiffness per unit area / (N/m^3)	1.5e+06
Critical normal stress of the outer layer / Pa	25000
Critical tangential stress of the outer layer / Pa	15000
Critical normal stress of the inner layer / Pa	23000
Critical tangential stress in the inner layer / Pa	13000

TABLE 4. Particle contact coefficients.

Contact particles	Coefficient of recovery	Coefficient of static friction	Coefficient of kinetic friction
Soil–Soil	0.2	0.4	0.3
Soil–Claw finger	0.3	0.5	0.05
Soil–Grass roots	0.6	0.6	0.3
Grass roots–Claw finger	0.5	0.58	0.01
Grass roots–Grass roots	0.8	0.8	0.8

To improve the calculation efficiency, with reference to the agronomic parameters of corn planting and the distribution range of weed roots, the simulation area was set at 100 mm long × 80 mm wide × 80 mm high, and the generation mode was dynamic generation. To ensure that the generated soil particles were uniformly distributed, the following parameters were used: soil particle factory generation speed, Z = −0.5 m/s; gravity direction, Z = −9.81 m/s^2; grass root number, 1; and descending speed, Z = −0.1 m/s. According to the order from the inside to the outside, the inner layer of soil was stabilised to generate the grass root particles and to bury the grass roots, and the external soil was generated to complete the establishment of the root–soil discrete meta-model. The total number of particles generated by the particle factory in the cube was 9,371,364 particles, and the distribution of the particle size in accordance with sieving was 1,124,564, 1,967,986, 4,591,968, 1,218,277, and 468,569 in descending order. The generated soil model is shown in Figure 5.

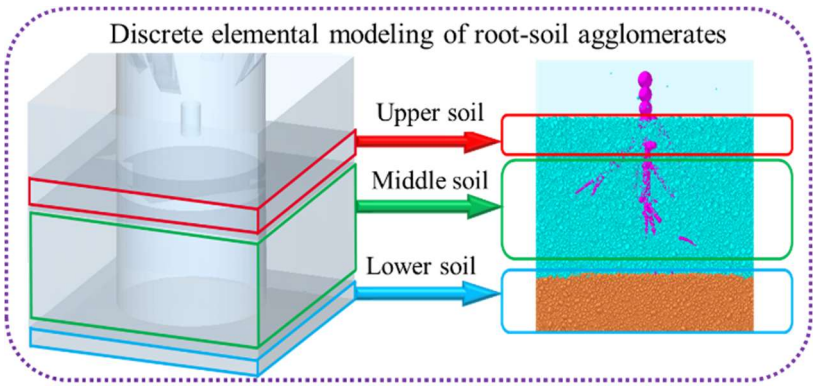

FIGURE 5. Discrete elemental model of agglomerates.

Bionic claw finger design

Claw toe contour curve extraction and fitting: The crab claw toe was placed on a solid colour background using a camera to photograph the crab claw toe. As shown in Figure 6, the crab claw toe image was transformed into a mathematical model through Matlab software image processing techniques. The original image of the crab claw toe was grey scaled and transformed into a binarised image. The noise was eliminated, and the residual parts were filled in through the expansion and erosion process Zhang (2015). The edge profile was extracted using the command to remove the edge profile for the contour curve of the crab's claw toe, and finally, the coordinate points of the required contour part were selected according to the user's customisation and fitted to determine the accurate coordinate equation of the contour of the claw toe.

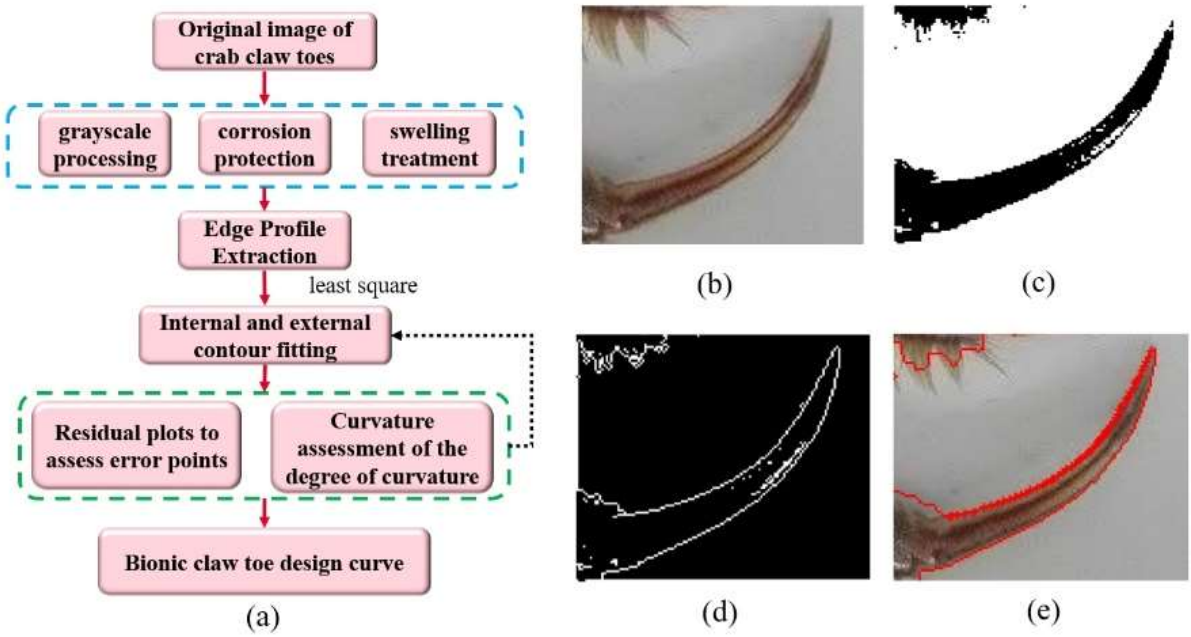

FIGURE 6. Claw toe curve extraction process. (a), Logic block diagram. (b), Original image. (c), Binarised image. (d), Extraction of the contours. e, Selection of contours.

The least squares method was used to fit the data, and the R_2 value assessed the degree of curve fitting, and the group with the best fitting effect was selected as the basis for the design. The third claw toe (R_2 = 0.999) had the most appropriate effect and could be used as the design parameter equations for the bionic claw finger, as shown in Figure 7. The fitted curve equations are as follows:

Inner contour curve equation:

$$f(x_1) = -2.35x^3 - 9.727x^2 - 21.36x + 59.21$$

The interval values were $45 \geq x_1 \geq 110$.

Equation of the outer contour curve:

$$f(x_2) = -5.475x^3 - 15.32x^2 - 25.63x + 70.74$$

The interval values were $65 \geq x_2 \geq 110$.

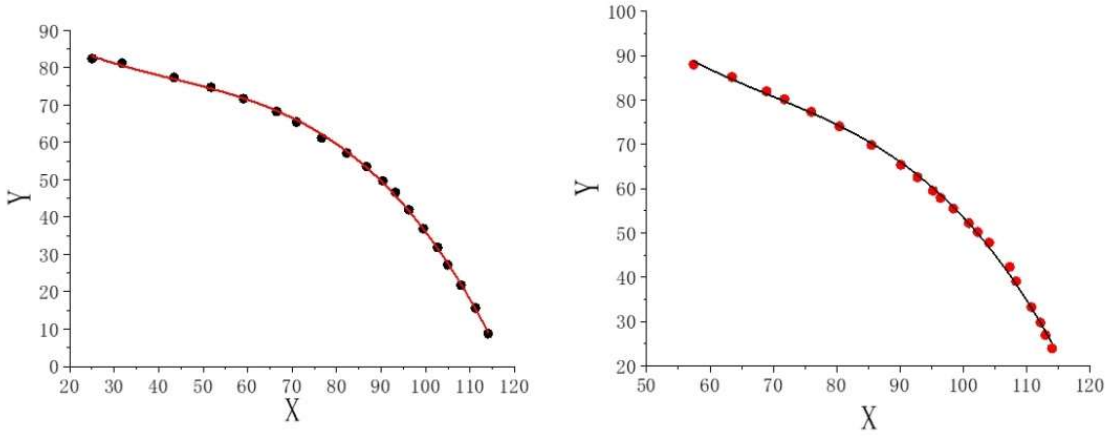

(a) Inner contour fitting curve (b) Outer contour fitting curve

FIGURE 7. Parameters of claw toe dimensions.

Three-dimensional modelling of claw fingers: The bionic claw finger structure was designed in Solid works based on the fitted curve equations, as shown in Figure 8, and divided into two parts, the working area and the installation area. The installation area was used for the installation of the claw finger, with the installation of the fixation of the six degrees of freedom through the setting of the two through holes with a diameter of 3 mm with the use of the bolts' constraints. The working area of the design parameters included the claw finger working length, the cutting edge angle of the tension angle, the width of the claw finger, the thickness of the claw finger, and the inner and outer surfaces of the angle of the tension angle. The inner contour line of the crab's claw toe was the inner surface bus of the bionic claw finger, and the outer contour line of the claw toe was the outer surface bus of the bionic claw finger. The claw finger will enter the soil in a cutting way when touching the soil, and a reasonable setting for the fingertip edge angle will help to break the soil when it touches (Yang et al., 2019; Zhao et al., 2024). It will be subjected to the soil pushing force on the inner surface of the claw finger when it cuts into the soil, and setting a certain surface tension angle will help to loosen the flow of the soil to the two sides to achieve the goal of reducing the drag force. The 3D model of the bionic claw finger is shown in Figure 8.

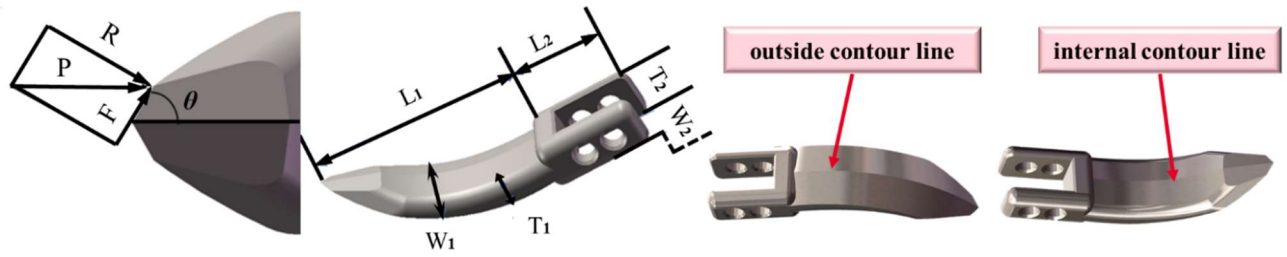

a. Cut edge tension angle b. Claw finger dimensions c. Outer contour curves d. Inner contour curves

FIGURE 8. 3D model of claw fingers.

Kinematic analysis of the working process of the gripper finger

Working principle of the gripper finger: To pull weeds using the bionic claw, the mechanism and working principle of pulling weeds needs to be fully understood (Dong et al., 2022). As shown in Figure 9, the claw finger begins to enter the soil to pull weeds through four stages: touching the soil, entering the soil, digging, and holding up the rise. To maintain a certain angle of entry into the soil, in the touching the soil stage, the bionic claw must contact and cut into the soil; then, in the entering the soil stage, the bionic claw fingers continue to cut deeply into the soil, destroying the stable structure of the soil agglomerate. In the digging stage, the bionic claw fingers continue to go deeper and push the internal soil to the middle of the aggregation, and the majority of the soil will be along the claw fingers and gaps in the flow, reducing resistance of the soil caused by the transfer. In the lifting stage, the remaining agglomerates are lifted after discharging the soil particles to detach the soil .

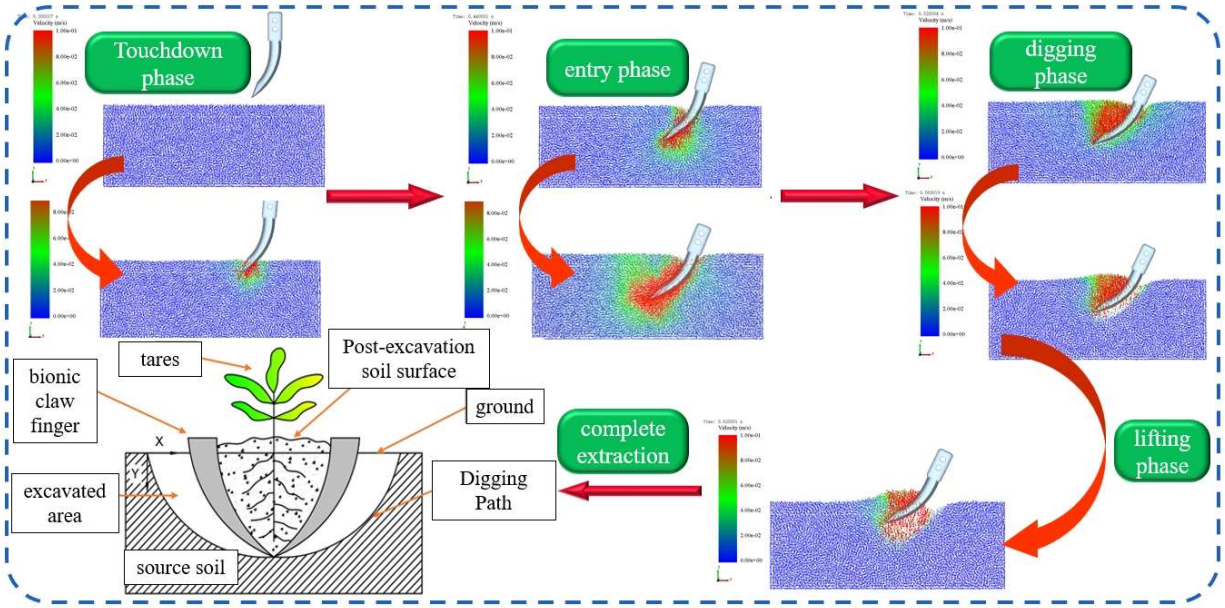

FIGURE 9. Working principle of the claw finger.

Bionic claw kinematic mechanism analysis: According to the working principle of the bionic claw finger, the mechanical claw body structure was designed to drive the movement of the bionic claw finger. The specific structure, including base, connecting rod, fixed rod, and other components, is shown in Figure 10a. As shown in Figure 10b in the mechanism sketch, can be determined by the principle of movement between the components (Nørremark et al., 2012; Pérez-Ruíz et al., 2014). The slider movement for the moving vice was set between the connecting rod for the rotation of the vice. Specific parameters are shown in Table 5. The number of moving parts, total number of high vices, and total number of low vices were determined to calculate the degrees of freedom, as follows:

$$F = 3n - 2P_L - P_H \quad (2)$$

Where:

n - number of active members;

P_L - number of low subs;

P_H - number of high subs.

Therefore, since the slider is the only prime mover member that has one degree of freedom to move in the Z direction and is constrained by the other five degrees of freedom, it has deterministic motion (Bawden et al., 2017). It is possible to control the opening and closing motions of the gripper jaws by controlling the motion of the slider.

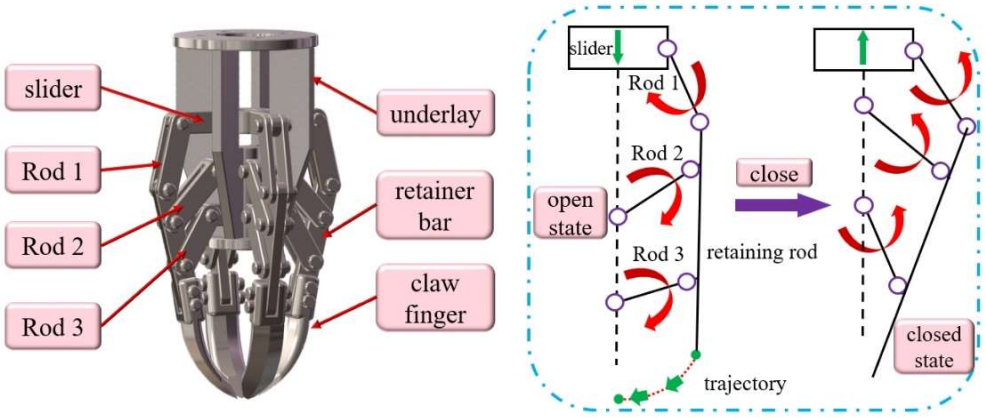

a. Composition of the gripper structure

b. Sketch of the gripper movement

FIGURE 10. Working principle of the claw finger.

TABLE 5. Particle contact coefficients.

Name of component	Sports vice	Quantities
Slider - Base	moving partner	1
Base - Ground	fixed constraints	1
Claw finger - Fixing lever	fixed constraints	1
Rod 1 - Fixed rod	rotating partner	1
Rod 1 - Base	rotating partner	1
Rod 2 - Base	rotating partner	1
Rod 2 - Fixed rod	rotating partner	1
Rod 3 - Base	rotating partner	1
Rod 3 - Fixed rod	rotating partner	1

Analysis of the resistance of the claw finger entering the ground

The bionic weeding claw finger, which is in direct contact with soil parts, will produce mutual contact and relative slippage in the process of working with the soil; this phenomenon will produce several forces on the bionic claw finger into the soil and on the soil disturbances caused by the situation (Ma et al., 2021; Wang et al., 2021). Its main forces consist of the cutting resistance of the claw tip to the soil, the push resistance of the inner wall of the claw to the soil, the friction of the soil on the inner and outer side walls of the claw finger, and the adhesion resistance between the soil and the claw finger. These are discussed separately below.

The working resistance is described, and the total resistance to entry is calculated as follows:

$$R = F_1 + F_2 + F_3 + F_4 \quad (3)$$

Where:

F_1 - cutting edge cutting resistance (N);

F_2 - inner horizontal nudge resistance (N);

F_3 - friction resistance (N);

F_4 - adhesion resistance (N).

Cutting resistance at the edge: The bionic claw edge cutting resistance to soil is an important part of operational resistance. Unlike the shovel-digging process, which fails the soil as a whole, the cutting action affects the soil with small and localised failure and breakage Chang (1981). The resistance of the cutting edge to cutting during the weeding operation was analysed and studied separately.

$$F_1 = C_1 e^{c_2 a_m} \cdot K_f \cdot C_3 \Delta\rho + \Delta F_{RB} + \Delta F_{Rh} + \Delta F_c \quad (4)$$

Where:

F_1 - cutting edge cutting resistance (N);

a_m - calculated particle size of soil (mm);

K_f - soil particle shape factor (N);

Δ_ρ - soil density (kg/m^3);

ΔF_{RB} - resistance increment with edge width (N);

ΔF_{Rh} - resistance increment with depth of cut (N);

ΔF_c - increment of resistance to change in the number of cut grass roots (N).

The increment of drag that varies with edge width and depth of cut is:

$$\Delta F_{RB} = C_4 e^{c_5 a_m}(B - 900)$$

$$\Delta F_{Rh} = C_6 e^{c_7 a_m}(H - 300)$$

Where:

$C_1 = 0.14$, $C_2 = 0.019$, $C_3 = 1.26$, $C_4 = 2.1\times10^{-2}$, $C_5 = 0.017$, $C_6 = 1.21\times10^{-2}$, $C_7 = 0.0145$

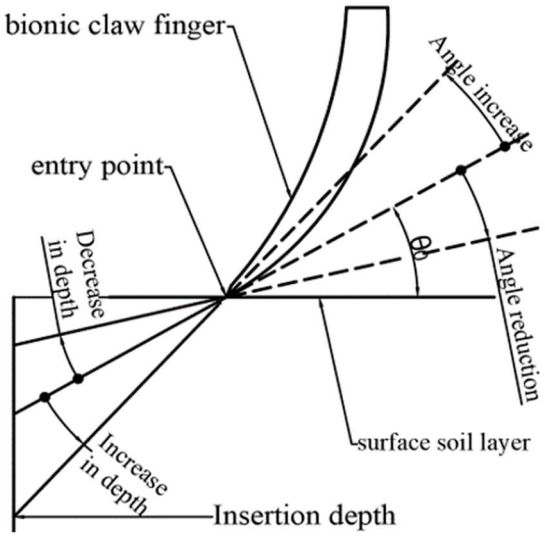

FIGURE 11. Model of cutting resistance at the cutting edge.

Inside horizontal push resistance: When the soil and bionic claw finger come into contact, the most influential resistance is the inner horizontal push resistance during bionic claw operation (Zhang et al., 2022). In the soil, the agglomerate structure of pressure particles is adjusted. The interface shape tends to comply with the interface shape of the component material. In the grasping process, all claw fingers and the region of contact with the soil are subjected to the action of the soil pressure. This study assumes that the bionic claw finger in the grasping operation is only subjected to the inner horizontal push resistance, the effective calculation of the contact area for the actual contact area in the horizontal direction of the projections. Since it is difficult to determine the exact height of soil accumulation on the claw fingers, the depth of grapple cut-in H_X is approximated instead (Xu et al., 2015). According to the theory of Coulomb soil mechanics, at the depth of incision H_X, the local soil agglomerate structure is destabilised by the bionic claw finger, producing the slip-cut phenomenon. At this time, the bionic claw finger is subjected to inward nudging resistance, which is mainly composed of the horizontal resistance to the movement of the soil agglomerate at the slipping surface, R_1, and the horizontal resistance to the destabilised agglomerate, R_2, as calculated by the following formula:

$$F_2 = R_1 + R_2 \quad (5)$$

The horizontal resistance R_1 generated by the movement of soil aggregates at the slip surface is determined as follows:

$$R_1 = G_1 \cdot tan[\theta + \varphi_0] \quad (6)$$

Where:

G_1 - soil aggregate Δabd gravity (N);

φ_0 - angle of the internal friction of the soil (°);

β - angle between the virtual working plane of the claw finger and the vertical line (°);

θ - soil slip angle (°), $45° - (\varphi_0 - \beta) / 2$.

In the process of grasping, the inner side of the bionic claw fingers that is in contact with the soil is subjected to the pressure action of the soil, according to the theory of Coulomb geotechnics, which is the magnitude of the passive soil destabilised agglomerate pressure at a depth of incision H_X. This can be calculated as follows:

$$P_p = K_p \cdot \gamma_m \cdot H_X + 2c \cdot \sqrt{K_p} \quad (7)$$

Where:

K_P - passive soil pressure coefficient;

γ_m - soil capacity;

C - soil cohesion (KN/m^2).

The passive soil pressure coefficient, K_p, can be expressed as a function of the angle of internal soil friction, as follows:

$$K_p = tan^{\,2}(\frac{\pi+\varphi_0}{2}) = cot^{\,2}\theta \quad (8)$$

The horizontal projection of the contact area of the soil and the bionic claw finger is the effective calculation area of the thrust resistance. The magnitude of the horizontal resistance R_2 of the Δbcd destabilised agglomerates at the inner contact surface of the claw finger can be obtained by integrating the horizontal projection as follows:

$$R_2 = \int_0^{H_X} P_p \cdot BdH = B \cdot (\frac{1}{2}K_p \cdot \gamma_m \cdot {H_X}^2 + 2c \cdot H_X \cdot \sqrt{K_p}) \quad (9)$$

Friction and adhesion resistance: The frictional resistance of the claw finger is the tangential resistance of the soil when tangential relative slip occurs along the contact interface of the claw finger. As the contact area between the surface material and the soil before and after the claw finger into the soil increases creep or plastic contact occurs due to the squeezing out of the dirty layer, and sometimes there may be intermittent slipping and sticking, thus increasing the resistance. Friction and adhesion of the soil are influenced by factors such as soil moisture content and material surface properties, and adhesion and friction are generally linearly related to positive pressure (Mu et al., 2023). In general, as the pressure between the soil and the material increases, the actual contact area between the soil and the material also increases. Therefore, the resulting adhesion and friction is greater. The following equations can be used to calculate the theoretical friction between the soil and claw fingers:

$$F_3 = R_3 + R_4 \quad (10)$$

$$R_3 = G_{\text{II}} \cdot cos\alpha_X \cdot tan\beta + F_2 \cdot sin\alpha_X \cdot tan\beta \quad (11)$$

$$R_4 = C_a + \sigma_n tan\varphi_0 = (C_{at} + C_{an} + \sigma_n)\, tan\varphi_0 \quad (12)$$

Where:

R_3 - tangential sliding friction resistance of the inner contact surface (N);

R_4 - tangential sliding friction resistance of the outer contact surface (N);

C_{at} C_{an} - unit faces normal force of attachment (N);

σ_n - normal specific pressure on the friction surface (N).

The frictional resistance of the claw finger is divided into two parts: one is the frictional resistance caused by the static pressure of the soil on the outside of the claw toe, R_3; and the other is the frictional resistance caused by the soil sliding in on the inside of the claw finger, R_4. The magnitude of both is affected by the mechanical properties of the soil and the surface condition of the claw toe. The adhesion of the soil to the bionic claw finger, i.e., the tensile strength in the vertical direction of the joint surface between the soil and the claw finger, is expressed by F_4, as calculated in the following equation:

$$F_4 = \frac{P}{S} \quad (13)$$

Where:

P - force applied vertically along the bonding surface (N);

S - contact area between the claw finger and soil (mm^2).

It is generally recognised that the adhesion between the soil and the contact material is determined by the following five forces. This was calculated as follows:

$$P = q_M + q_E + q_K + q_B - q_P \quad (14)$$

Where:

q_M - gravitational force between molecules (N);

q_E - electrostatic attraction between soil and claw body (N);

q_K - water tension (N);

q_B - soil and contact material viscous resistance (N);

q_P - wedge opening force (N).

The effects of these five forces on adhesion differ depending on the soil conditions. Among them, the one that plays a decisive role in soil adhesion is the water tension, q_K, generated by the water film between the soil and material surface.

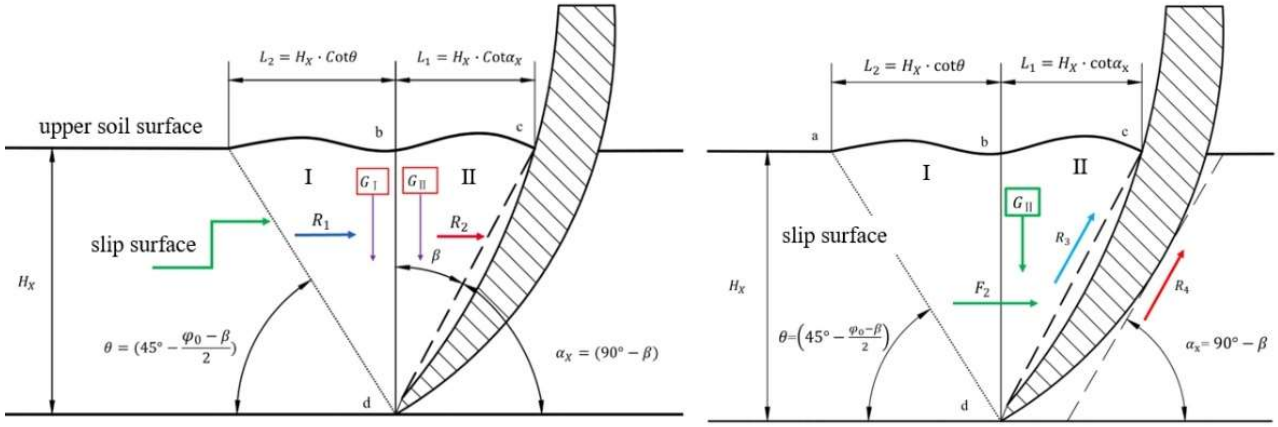

a. Inside horizontal nudge resistance modelling b. Claw finger friction resistance model

FIGURE 12. Force distribution schematic.

RESULTS AND DISCUSSION

Results of kinematic analysis of the working process of the claw finger

Based on the type and number of motion subs between each component (Table 5), Recur Dyn software was used to carry out multi-body kinematics simulation of the mechanical clamping claw, setting the base as a fixed part, the slider as a prime mover, and the range of the moving distance at 35 mm, marking the marker points on the tip of the bionic claw finger to statistically count the claw finger movement, and setting the simulation solution time as 1s and the time step as 100. The gravity was Z = −9806.65 mm/s^2, and multi-body kinematics simulation was performed on the mechanical claw.

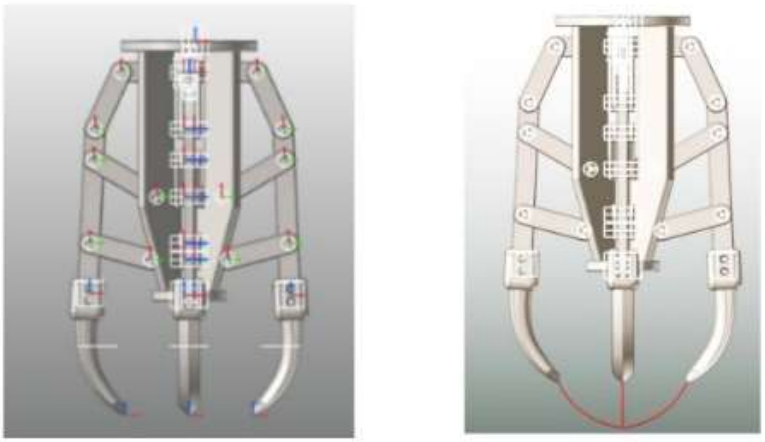

a. Motion sub-imposed b. Bionic claw finger trajectory

FIGURE 13. Pretreatment of the mechanical claw.

Through the mechanical claw motion simulation of the bionic claw finger trajectory, as shown in Figure 13b, claw finger trajectory and the expected claw finger trajectory was in line with the confirmation of the structure to meet the expected work requirements. On the bionic claw finger, marker point displacement changes were analysed. Due to the axisymmetric structure of the mechanical claw, the individual claw finger movement was the same, and in this study, only one of the claw fingers was analysed. As shown in Figure 14 a and d, in the X direction, the displacement of the claw finger closed was −20 mm at 0–0.4 s and opened was 20 mm at 0.4–0.7 s. In the Z direction, the displacement of the claw finger closed was −35 mm at 0–0.4 s and opened was 35 mm at 0.4–0.7 s, as shown in Figure 14 b and d. The total motion of the claw finger can be described as follows. Figure 14c and d shows the total movement of the claw finger, which can be described as follows: at 0–0.3 s, the claw finger first slowly accelerated down to near the end position; at 0.3–0.4 s, it decelerated down to finally reach the closed position. This change was to ensure that the claw finger was stable and closed and that it did not collide, as it would if the speed was too high. At 0.4–0.5 s, the claw finger accelerated to open to facilitate the rapid release of the seized weed, and at 0.5–0.7 s, it slowed to open. The Z direction displacement was −35 mm, as shown in Figure 14b. At 0.7 s, it changed to a slow deceleration movement, and the claw finger finally reached the maximum opening and closing position with a stable movement state.

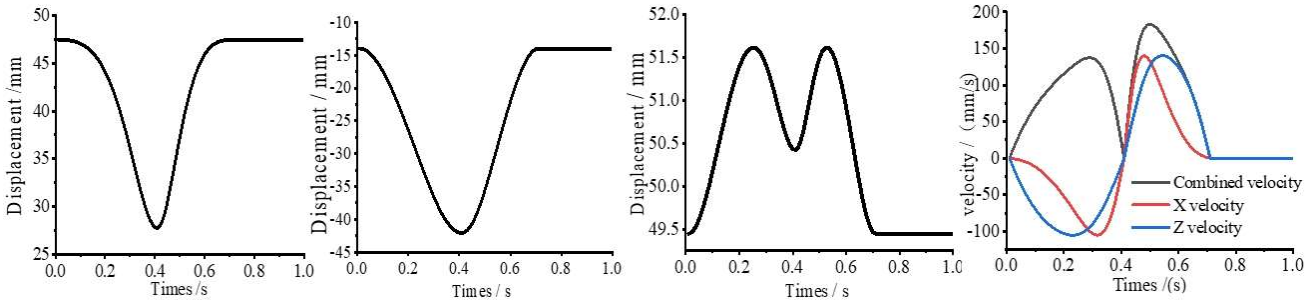

a. X direction displacement b. Z direction displacement c. Total displacement d. Velocity variation

FIGURE 14. Movement of the claw fingers.

Simulation analysis of the working process of the bionic weeding claw

At this stage, the use of mechanical claws to pull the weeds out of the weed control device is reduced. There is a lack of mutual comparison for the test object. This study adopted the flat claw finger as a comparative object to fully realise the bionic claw in the working process of its structural advantages, with the soil flow rate, soil displacement state, soil disturbance rate, and the force of the grass roots, and resistance of the claw finger entering the soil as the test objectives for the simulation of the comparison test. To ensure the accuracy of the test to reduce error, the flat claw finger and bionic claw finger design parameters were set to be basically the same. The design parameters (length, width, thickness) were as follows: 40 mm × 10 mm × 10 mm; cutting edge of the tension angle, 80°; angle of entry into the soil, 70°; number of claw fingers, 4; and same drive structure as the bionic claw fingers. The 3D model produced using Solid works modelling is shown in Figure 15.

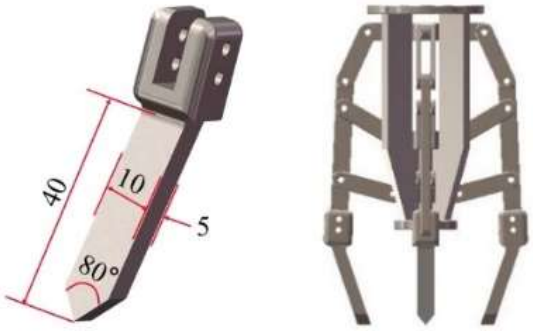

FIGURE 15. Three-dimensional model of flat jaw finger and mechanical jaws.

A comparative test of the gripping process: Based on the MBD-DEM (Dynamics of Multi-body System and Discrete Element Method) joint simulation test to simulate the work of a bionic mechanical claw pulling weeds, the mechanical claw 3D model was converted to igs format and imported into Recur Dyn software. The motion vice and constraints were set, and the slider, which was the moving part, had a movement distance of 35 mm. The length of time was 0.4 s, and the four claw fingers were saved as a wall file and exported. The root–soil generated in the previous section was used as a model for the root–soil. The discrete element model was opened in EDEM and imported into the wall file. The simulation time of the both software was set to 1 s, and the saving step was set to 0.01 s. To facilitate the observation of the internal particle movement, the simulation test model was sliced and dissected, as shown in Figure 16.

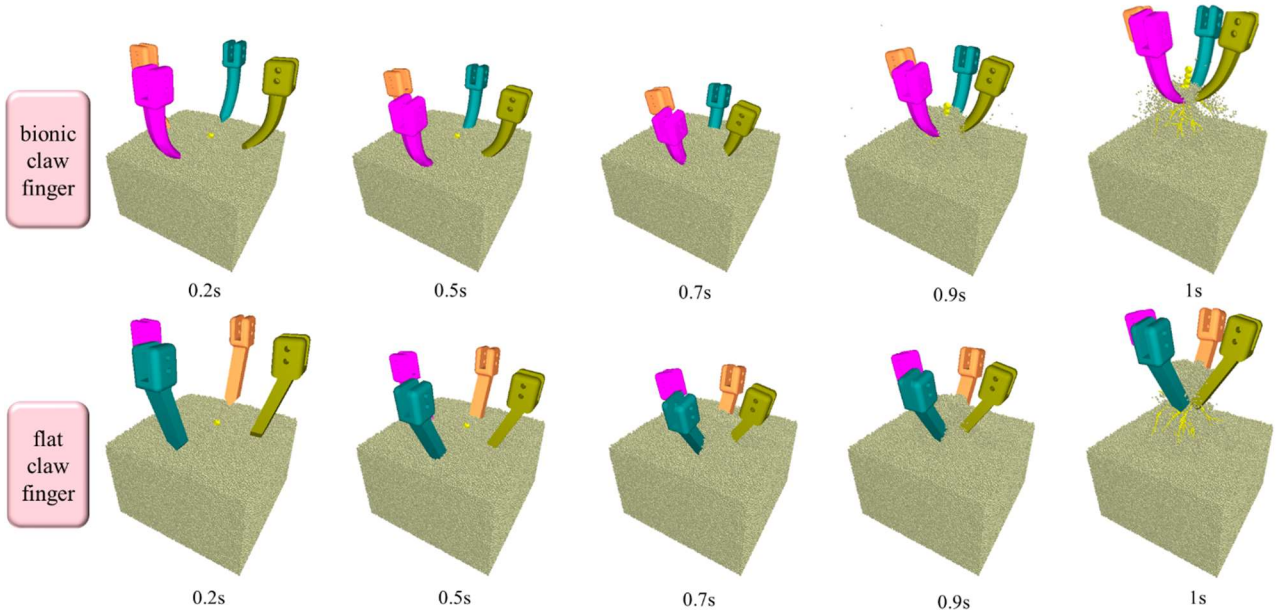

FIGURE 16. Joint simulation of the grasping process.

As shown in Figure 16, when the mechanical claw makes the downward movement to the near ground, the bionic claw fingertips are gradually inserted into the soil, with the claw finger just entering the soil. Due to the claw finger cutting edge of the shear and the inside and outside of the curved surface extrusion, the soil become displaced and the speed changes. The claw finger continues to move deeper, and the cutting edge of the soil carries a continuous shear. The soil is divided into the upper and lower parts of the inner surface of the push and pressure. Due to the degree of bending, in the inner surface, which has a role in the angle of tension and moves the soil upward, the inner wall is gradually shunted to two sides to avoid the phenomenon of congestion and to reduce the resistance of the push. Due to the claw finger, the whole form is gradually thicker from the bottom up, with the claw finger deep inside along the inner wall, and climbing a distance occurs after the broken fracture phenomenon. When it reaches the maximum depth of contact, wrapping the grass roots and the main root system, the claw body rises to completely pull out the weed's root system. Compared with the bionic claw finger, after the flat claw finger enters the soil, with the increase in the soil depth, the soil gradually accumulates on the inner surface of the claw finger. The congestion phenomenon is serious, making the excavation resistance increase so that the bionic claw finger can effectively solve the congestion problem when pulling out the weeds and keeping the roots of the grass intact to the maximum extent when pulling out the grass roots.

Comparison test of soil particle displacement and movement velocity: Under the action of different claw fingers, the soil and root complexes are damaged in different ways; the claw finger in the deep soil layer experiences extrusion and shear, crushing soil particles to obtain a certain speed of movement. The nonlinear displacement changes of the claw finger are shown in Figure 17. Although movement speed changes are observed for the particles, the bionic claw finger inside the contour of the curved curves. The curved surface tensor angle structure enables the soil particles to flow along the angle of the tensor. Both sides of the surface flow, reducing the direct push resistance and friction. In the simulation test post-processing module for different positions, different soil layers of soil particles were marked to analyse the changes in the locations of these particles, speed, and distribution of the claw finger after contact with the claw finger.

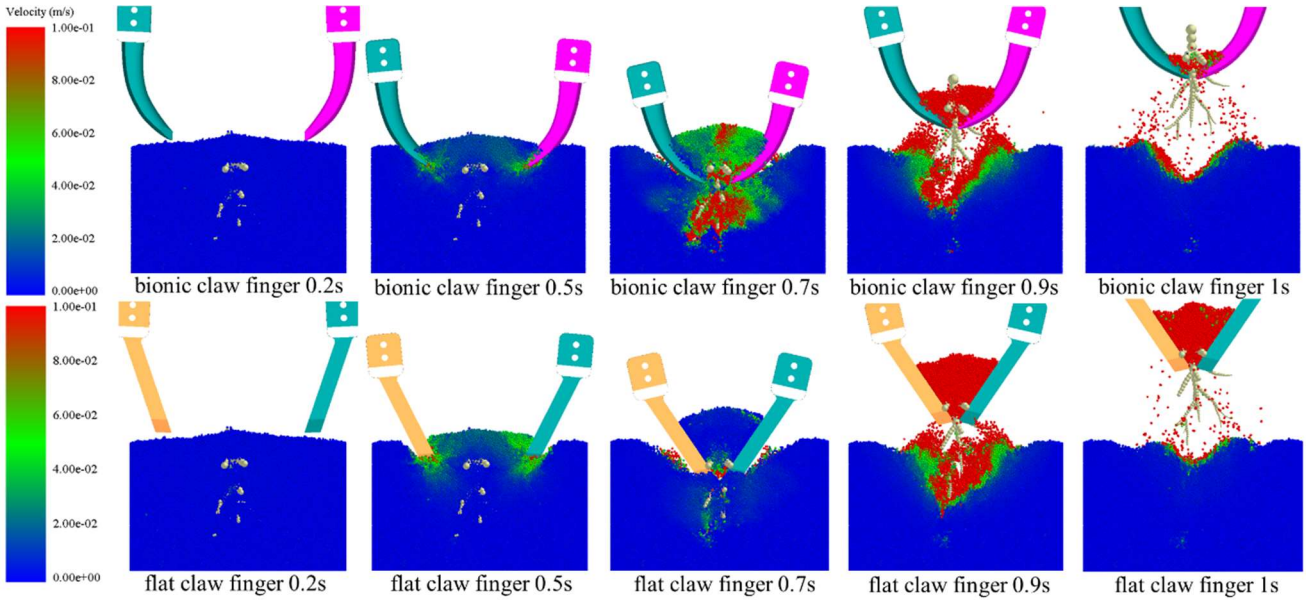

FIGURE 17. Velocity distribution of soil particle movement.

According to the soil particle factory generated above, in the slicing process of the post-processing module, the slice thickness and claw finger width were 10 mm in the sliced soil particles. The inner side of the outer layer of the claw finger and inner layer of the soil particles, which were in contact, were labelled and numbered, as shown in Figure 17. Based on particle movement displacement statistics, the trajectory of its movement along the claw finger tensor surface to the displacement of the particles was determined, and the trajectory of the particles was along the surface of the claw finger tensor surface to both sides. Compared with the displacement of the soil particles of the bionic claw finger, the soil particles under the action of the flat claw finger were more piled up along the surface of the claw finger, resulting in smaller displacement, which indicated that the bionic claw finger was more likely to disturb the soil than the flat claw finger. It has a positive effect on reducing the resistance of entering the soil, as shown in Figure 18.

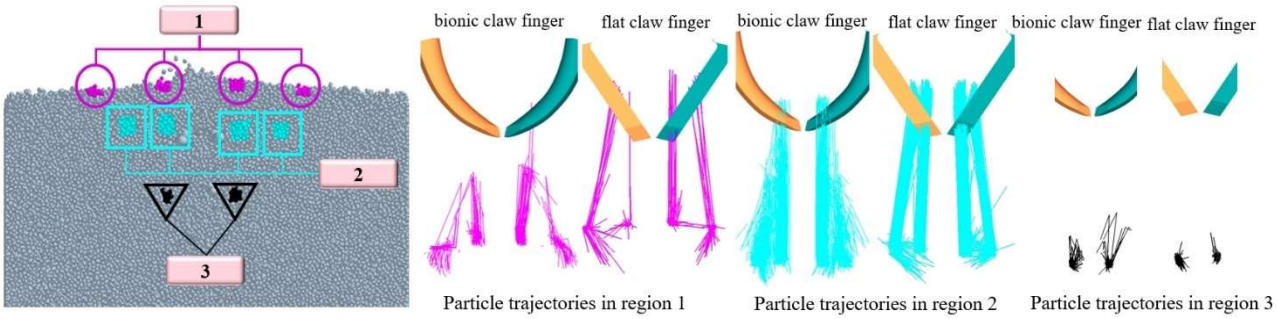

a. Soil particle labelling serial numbers

b. Soil particle movement trajectories

FIGURE 18. Soil movement marking results.

Comparative stress test of grass roots: In the simulation test post-processing interface, the grass root force situation was statistically analysed. As shown in Figure 19 a, the grass root has a total several times that of the force change. At 0.2–0.65 s, within the weed root system, there is shear action from the cutting edge of the claw finger, and soil displacement occurs under the tensile action of the grass roots. At 0.65–0.7 s, the claw finger continues to reach for the deepest depth of the grass roots, causing force to reach its first peak. At this time, grass root agglomerates due to claw finger interference, and internal claw finger agglomerates on the soil layer gradually rupture due to the main factor of force for the root–soil agglomerates, which is the tensile force. The flat claw finger cutting edge width is wider than the bionic claw finger, indicating more root-soil agglomerates and the occurrence of shear action. At 0.7–0.75 s, the stress on grass roots turned increased and reached the second peak, and the claw finger reached a maximum depth and was in the state of complete closure. The stress on grass roots was obviously higher than that using the bionic claw finger under the action of the closed claw finger, indicating that the bionic claw finger could disturb and loosen the soil very well. The stress on grass roots was smaller, with less soil compression inside the claw finger. At 0.75–0.8 s, the force on the grass roots peaked again, indicating that under the action of the claw finger, the root system detached significantly from the internal soil, the stabilised agglomerates became loose, and the generated agglomerative force began to be less than the grasping force of the claw finger. At 0.8–0.1 s when the grass roots are grasped by the claw finger and gradually moved to

the outer layer of soil, the main root system are subject to the friction between the soil particles. The interaction between the grass roots and the soil depth gradually become shallower. The friction between the grass root and the soil particles is also gradually reduced until the grass root is completely pulled out. At this time, the grass root stress tends to be stabilised due to the effect of the bionic claw finger on soil perturbation. Grass roots are not easy to break, more to ensure the integrity of pulling out. Due to the disturbance and loosening effect of the bionic claw finger on the soil, the friction between the grass root and the soil in the process of detaching from the soil is smaller than that of the flat claw finger, as the grass root system is not easy to break. The completeness of the root is guaranteed.

Comparative test of claw finger in-ground resistance: According to the claw finger force model, the main force composition of the claw finger for cutting resistance, push resistance, friction, and adhesion resistance in the claw finger cannot measured separately. This study measured and comparatively analysed the average ground resistance of the claw finger. The average change in the ground resistance is shown in Figure 19b. Due to the excellent characteristics of the bionic claw finger, its resistance in entering the ground is much lower than that of the flat claw finger. The average resistance reduction rate is 16.4%.

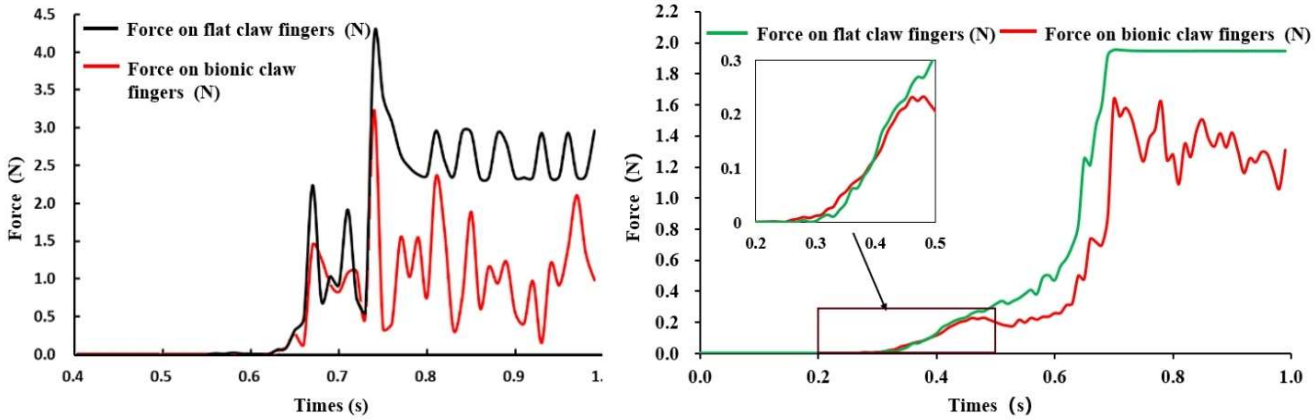

a. Force on grass root

b. Force on claw finger resistance to entry soil

FIGURE 19. Target force conditions.

CONCLUSIONS

Based on Matlab image processing technology, the inner and outer contour curves of the crab claw toe were extracted, which were fitted as a bionic design prototype, and a 3D model of the bionic claw finger was established. Based on the single image inverse reconstruction technology, a simulation model of the weed root system was obtained, and the discrete element particles were filled in. According to the mechanical soil dynamics theory of the kinetic analysis of the bionic claw finger weeding process, the bionic claw finger was used for weed removal. The resistance in the process consisted of cutting resistance, inner horizontal push resistance, friction resistance, and adhesion resistance.

From the kinematics simulation test, the claw finger must touch the soil, from the beginning of entering the soil to pulling out the weed, going through four stages: entering the soil, into the soil, digging, and lifting. The working principle of the mechanical claw is basically realised. There is no dead point of movement, and the movement state is stable. Through the calculation of the degrees of freedom, it was concluded that the mechanism has a deterministic movement, and through the marking of marker points on the tip of the claw finger, it is concluded that the claw finger trajectory is consistent with the expected working trajectory of the claw finger, which is consistent with the expected trajectory of the claw finger. By marking marker points on the tip of the bionic claw finger, the trajectory of the bionic claw finger is consistent with the expected trajectory of the claw finger, indicating that the bionic weeding claw movement meets the expected working requirements.

As shown in the joint simulation and comparison test, the tensor surface structure of the bionic claw finger can make the soil particles move along the contour line to both sides, which can reduce the push resistance, friction resistance, and adhesion resistance generated by the soil on the bionic claw finger, having a good crushing, loosening, and diversion effect. The combination of the bionic contour curve structure can inhibit congestion phenomenon with the increase in the amount of soil feeding. The piled up soil climbs along the contact surface, and the soil can be removed from the contact surface. The piled up soil along the contact surface is hindered from climbing, breaking the soil structure. The resistance of the process of entering the soil is reduced. According to the claw finger force situation of the bionic claw finger and flat claw finger compared to the average reduction rate of 16.4%, the force of the grass roots is reduced by 23.3%. It is easier to pull out more intact roots, in favour of the eradication of weeds in maize fields.

The bionic weeding claw can realise rapid positioning and precise weeding under the mutual cooperation of the mounting platform, machine vision, and weeding drive components; by changing or increasing the target crops for identification and protection, the bionic claw can also be used for weeding operations of crops such as cabbage and leafy green vegetables. Furthermore, weed eradication operations are needed to provide theoretical support.

ACKNOWLEDGMENTS

The authors would like to gratefully acknowledge the Inner Mongolia Autonomous Region Key R&D and the

Achievement Transformation Programme Project (Grant Nos.2022YFHH0122). The authors would like to thank the editors and reviewers for their valuable comments and constructive suggestions.

REFERENCES

Bawden O, Kulk J, Russell R, McCool C, English A, Dayoub F, Lehnert C, Perez T (2017) Robot for weed species plant-specific management. Journal of Field Robotic 34(6):1179-1199. https://doi.org/10.1002/rob.21727

Bo BC, Zhang S, Liu W, Liu L (2022) Simulation of workspace and trajectory of a weeding mechanism. Alexandria Engineering Journal 61(2):1133-1143. https://doi.org/10.1016/j.aej.2021.06.100

Cao CM, Liu ZB, Ding WY, Wu MY, Zhang XC, Qin K (2023) Design and experiment of Ning-guo Radix peucedani bionic digging shovel. Transactions of the Chinese Society for Agricultural Machinery 54(11):102-113. https://doi.org/10.6041/j.issn.1000-1298.2023.11.010

Chang QR (1981) On the gripping resistance of grab buckets. Journal of Shanghai Maritime University (02):43-61. DOI:CNKI:CDMD: 2.1015.594432.

Cordill C, Grift TE (2011) Design and testing of an intra-row mechanical weeding machine for corn. Biosystems Engineering 110(3):247-252. https://doi.org/10.1016/j.biosystemseng.2011.07.007

Dong XQ, Su C, Zheng HN, Han RQ, Li YL, Wan LPC, Song JN, Wang JC (2022) Analysis of soil disturbance process by vibrating subsoiling based on DEM-MBD coupling algorithm. Transactions of the Chinese Society of Agricultural Engineering (Transactions of the CSAE) 38(1): 34-43. https://doi.org/10.11975/j.issn.1002-6819.2022.01.004

Du W, Hai WB, Liu CY (2023) Design and analysis of bionic weeding wheel based on shell rib structure. Journal of Agricultural Mechanization Research 45(06):94-99. https://doi.org/10.13427/j.cnki.njyi.2023.06.005

Fan Y (2020) Research on potato digging mechanism based on discrete element method and design of bionic shovel. Shenyang Agricultural University. https://doi.org/10.27327/d.cnki.gshnu.2020.000039

Hai L, Tan SL, Xu B (2023) Mechanical properties of Medicago Sativa and Euphorbia Hypericifolia Root-Soil Complex. Bulletin of Soil and Water Conservation 43(06):57-64. https://doi.org/10.13961/j.cnki.stbcxb.2023.06.008

Li JW, Gu TL, Li XY, Wang ZJ, Hu B, Ma YH (2023) Analysis and experiment of the bionic drag reduction characteristics of potato digging shovels on clayey black soil conditions. Transactions of the Chinese Society of Agricultural Engineering (Transactions of the CSAE) 39(20): 1-9. https://doi.org/10.11975/j.issn.1002-6819.202305034

Liu JP, Zhou HY, He TK, Yu JN, Zhang K, Pan YC, Liu QS (2023) Experimental study on the influence of root content on the shear strength of root-soil-rock composite – taking Malus halliana koehne as an example. Chinese Journal of Rock Mechanics and Engineering 42(S1):3618-3628. https://doi.org/10.13722/j.cnki.jrme.2022.0053

Liu JY, Zhou ZC, Su XM (2019) Review of the mechanism of root system on the formation of soil aggregates. Journal of Soil and Water Conservation 34(03):267-273+298. https://doi.org/10.13870/j.cnki.stbcxb.2020.03.040

Liu ZH, Wu K, Guo JW, Wang YH, Oliver D, Cheng ZL (2021) Single image tree reconstruction via adversarial network. Graphical Models 117:101115. https://doi.org/10.1016/j.gmod.2021.101115

Ma WP, You Y, Wang DC, Hu JN, Huan XL, Zhu L. (2021) Design and experiment of low-resistance soil loosening shovel for cutting roots and reseeding in perennial alfalfa field. Transactions of the Chinese Society for Agricultural Machinery 52(02): 86-95+144. https://doi.org/10.6041/j.issn.1000-1298.2021.02.008

Mu GZ, Wang QY, Zheng DH, Li DS, Zhang TT, Zhang GC, Zhang WZ (2023) Design and experiment of the seedling planting device for a sweet potato horizontal multiple transplanter. Transactions of the Chinese Society of Agricultural Engineering (Transactions of the CSAE) 39(24): 1-10. https://doi.org/10.11975/j.issn.1002-6819.202306059

Nørremark M, Griepentrog WH, Nielsen J, Søgaard HT (2012) Evaluation of an autonomous GPS-based system for intra-row weed control by assessing the tilled area. Precision Agriculture 13(2):149-162. https://doi.org/10.1007/s11119-011-9234-5

Pérez-Ruíz M, Slaughter C D, Fathallah A F, Gliever CJ, Miller BJ (2014) Co-robotic intra-row weed control system. Biosystems Engineering 12645-55. https://doi.org/10.1016/j.biosystemseng.2014.07.009

Qi YC, Wang YQ, Liu J, Zhou C (2011) Comparative study on composition of soil aggregates with different land use patterns and several kinds of soil aggregate stability index. Transactions of the Chinese Society of Agricultural Engineering 27(01):340-347. https://doi.org/10.3969/j.issn.1002-6819.2011.01.055

Shen TL (2021) Development of corn industry and food security in China. Agricultural Economics (05):44-49. https://doi.org/10.3969/j.issn.1001-8573.2021.05.008

Tao ZW, Bu HY, Li JJ, Jia P, Qi W, Liu K (2021) Effects of different artificial planting schemes on invasive weeds. Global Ecology and Conservation (prepublish) e01651. https://doi.org/10.1111/j.1755-0998.2008.02546.x

Wang S, Su DBLG, Wang ZM, Jiang YY, Zhang LN, Tan Y (2021) Design and experiments of the cam swing rod intra-row weeding device for lettuce farm. Transactions of the Chinese Society of Agricultural Engineering 37(21): 34-44. https://doi.org/10.11975/j.issn.1002-6819.2021.21.005

Xiao MH, Wang KX, Yang W, Wang WC, Jiang F (2021) Design and experiment of bionic rotary blade based on claw toe of Gryllotalpa orientalis Burmeister. Transactions of the Chinese Society for Agricultural Machinery 52(02):55-63. https://doi.org/10.6041/j.issn.1000-1298.2021.02.005

Xu J, Liu BW, Chen PL (2023) Development and Experiment of vertical spiral cutter for soil loosening and weeding in Camellia oleifera forest. Transactions of the Chinese Society for Agricultural Machinery 54(12):79-87. https://doi.org/10.6041/j.issn.1000-1298.2023.12.007

Xu YL, Hu JQ (2015) Electric hydraulic dredging grab stress analysis on excavation process. Journal of Wuhan University of Technology 39(05):1079-1082+1086. https://doi.org/10.3963/j.issn.2095-3844

Yang RT, Ge RL, Hao XT, Wang ZX, Cui TM (2021) Comparison of composite shear mechanical properties of different types of soil-like caragana korshinskii Root. Chinese Journal of Soil Science 52(04):821-827. https://doi.org/10.19336/j.cnki.trtb.2020103101

Yang YW, Tong J, Ma YH, Jiang XH, Li JG (2019) Design and experiment of biomimetic rotary tillage blade based on multiple claws characteristics of mole rats. Transactions of the Chinese Society of Agricultural Engineering 35(19):37-45. https://doi.org/10.11975/j.issn.1002-6819.2019.19.005

Yin ZP (2022) Design and experimental study of bionic swipe shovel based on mole cave structure. Jilin University. https://doi.org/10.27162/d.cnki.gjlin.2022.004597

Zeng BG, Li M, Yao LH, Zhao SL, Chen X, Wang Y, Liu F, Xie SY (2023) Simulation and experiment on the mechanical properties of Coptis chinensis root-soil composites based on image reconstruction. Transactions of the Chinese Society of Agricultural Engineering (Transactions of the CSAE) 39(19): 75-84. https://doi.org/10.11975/j.issn.1002-6819.202305147

Zeng ZW, Ma X, Cao XL, Li ZH, Wang XC (2021) Critical review of applications of discrete element method in agricultural engineering. Journal of Agricultural Machinery 52(04):1-20. https://doi.org/10.6041/j.issn.1000-1298.2021.04.001

Zhang RR (2015) The biomimetic design on mars surface sampler and research on machine and soil's interaction. Jilin University. DOI:CNKI:CDMD: 2.1015.594432.

Zhang ZG, Xue HT, Wang YC, Xie KT, Deng YX (2022) Design and experiment of Panax notoginseng bionic excavating shovel based on EDEM. Transactions of the Chinese Society for Agricultural Machinery 53(05):100-111. https://doi.org/10.6041/j.issn.1000-1298.2022.05.011

Zhao SH, Zhao GP, Zhang X, Hou LT, Yuan YW, Yang YQ (2024) Design and experiment of weeding device between three rows of dense planting on soybean ridge. Journal of Agricultural Mechanization Research 1-10. https://doi.org/10.13427/j.cnki.njyi.20240019.018